A Study of Injection Locking and Pulling in Oscillators

Behzad Razavi, *Fellow, IEEE*

***Abstract*—Injection locking characteristics of oscillators are derived and a graphical analysis is presented that describes injection pulling in time and frequency domains. An identity obtained from phase and envelope equations is used to express the requisite oscillator nonlinearity and interpret phase noise reduction. The behavior of phase-locked oscillators under injection pulling is also formulated.**

***Index Terms*—Adler's equation, injection locking, injection pulling, oscillator nonlinearity, oscillator pulling, quadrature oscillators.**

INJECTION of a periodic signal into an oscillator leads to interesting locking or pulling phenomena. Studied by Adler [1], Kurokawa [2], and others [3]–[5], these effects have found increasingly greater importance for they manifest themselves in many of today's transceivers and frequency synthesis techniques.

This paper describes new insights into injection locking and pulling and formulates the behavior of phase-locked oscillators under injection. A graphical interpretation of Adler's equation illustrates pulling in both time and frequency domains while an identity derived from the phase and envelope equations expresses the required oscillator nonlinearity across the lock range.

Section II of the paper places this work in context and Section III deals with injection locking. Sections IV and V respectively consider injection pulling and the required oscillator nonlinearity. Section VI quantifies the effect of pulling on phase-locked loops (PLLs) and Section VII summarizes the experimental results.

I. General Considerations

Oscillatory systems are generally prone to injection locking or pulling. As early as the 17th century, the Dutch scientist Christiaan Huygens, while confined to bed by illness, noticed that the pendulums of two clocks on the wall moved in unison if the clocks were hung close to each other [6]. He postulated that the coupling of the mechanical vibrations through the wall drove the clocks into synchronization. It has also been observed that humans left in isolated bunkers reveal a "free-running" sleep-wake period of about 25 hours [7] but, when brought back to the nature, they are injection-locked to the Earth's cycle.

Manuscript received December 16, 2003; revised March 17, 2004.

The author is with the Department of Electrical Engineering, University of California, Los Angeles, CA 90095 USA (e-mail: razavi@ee.ucla.edu).

Digital Object Identifier 10.1109/JSSC.2004.831608

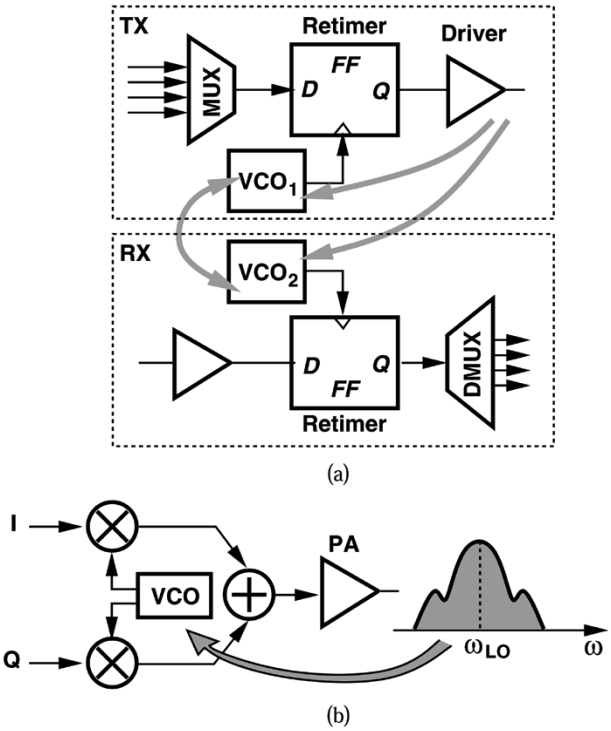

Fig. 1. Oscillator pulling in (a) broadband transceiver and (b) RF transceiver.

Injection locking becomes useful in a number of applications, including frequency division [8], [9], quadrature generation [10], [11], and oscillators with finer phase separations [12]. Injection pulling, on the other hand, typically proves undesirable. For example, in the broadband transceiver of Fig. 1(a), the transmit voltage-controlled oscillator, VCO_1, is locked to a local crystal oscillator whereas the receive VCO, VCO_2, is locked to the incoming data and hence potentially a slightly different frequency. Thus, the two oscillators may pull each other as a result of coupling through the substrate. Similarly, the high-swing broadband data at the output of the transmitter may pull VCO_1 and VCO_2 as it contains substantial energy in the vicinity of their oscillation frequencies.

Fig. 1(b) depicts another example of undesirable pulling. The power amplifier (PA) output in an RF transceiver contains large spectral components in the vicinity of ω_{LO}, leaking through the package and the substrate to the VCO and causing pulling.

II. Injection Locking

Consider the simple (conceptual) oscillator shown in Fig. 2, where all parasitics are neglected, the tank operates at the resonance frequency $\omega_0 = 1/\sqrt{L_1 C_1}$ (thus contributing no phase

0018-9200/04$20.00 © 2004 IEEE

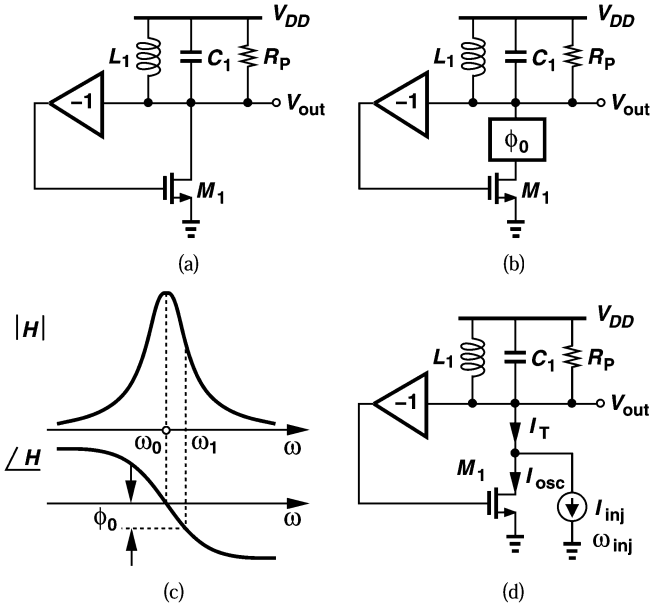

Fig. 2. (a) Conceptual oscillator. (b) Frequency shift due to additional phase shift. (c) Open-loop characteristics. (d) Frequency shift by injection.

shift), and the ideal inverting buffer follows the tank to create a total phase shift of 360° around the feedback loop. What happens if an additional phase shift is inserted in the loop, e.g., as depicted in Fig. 2(b)? The circuit can no longer oscillate at ω_0 because the total phase shift at this frequency deviates from 360° by ϕ_0. Thus, as illustrated in Fig. 2(c), the oscillation frequency must change to a new value ω_1 such that the tank contributes enough phase shift to cancel the effect of ϕ_0. Note that, if the buffer and M_1 contribute no phase shift, then the drain current of M_1 ($I_{\rm osc}$) must remain in phase with $V_{\rm out}$ under all conditions.

Now suppose we attempt to produce ϕ_0 by *adding* a sinusoidal current to the drain current of M_1 [Fig. 2(d)]. If the amplitude and frequency of $I_{\rm inj}$ are chosen properly, the circuit indeed oscillates at $\omega_{\rm inj}$ rather than at ω_0 and injection locking occurs. Under this condition, $V_{\rm out}$ and $I_{\rm inj}$ *must* bear a phase difference [Fig. 3(a)] because: 1) the tank contributes phase at $\omega_{\rm inj} \neq \omega_0$, rotating $V_{\rm out}$ with respect to the resultant current, I_T, and 2) $I_{\rm osc}$ still remains in phase with $V_{\rm out}$ and hence out of phase with respect to I_T, requiring that $I_{\rm inj}$ form an angle with $I_{\rm osc}$. (If $I_{\rm inj}$ and $I_{\rm osc}$ were in phase, then I_T would also be in phase with $I_{\rm osc}$ and thus with $V_{\rm out}$). The angle formed between $I_{\rm osc}$ and $I_{\rm inj}$ is such that I_T becomes aligned with $V_{\rm osc}$ (and $I_{\rm osc}$) after experiencing the tank phase shift, ϕ_0, at $\omega_{\rm inj}$.

In order to determine the lock range (the range of $\omega_{\rm inj}$ across which injection locking holds), we examine the phasor diagram of Fig. 3(a) as $\omega_{\rm inj}$ departs from ω_0. To match the increasingly greater phase shift introduced by the tank, the angle between $I_{\rm osc}$ and I_T must also increase, requiring that $I_{\rm osc}$ rotate counterclockwise [Fig. 3(b)]. It can be shown that

$$\sin\phi_0 = \frac{I_{\rm inj}}{I_T}\sin\theta \tag{1}$$

$$= \frac{I_{\rm inj}\sin\theta}{\sqrt{I_{\rm osc}^2 + I_{\rm inj}^2 + 2I_{\rm osc}I_{\rm inj}\cos\theta}} \tag{2}$$

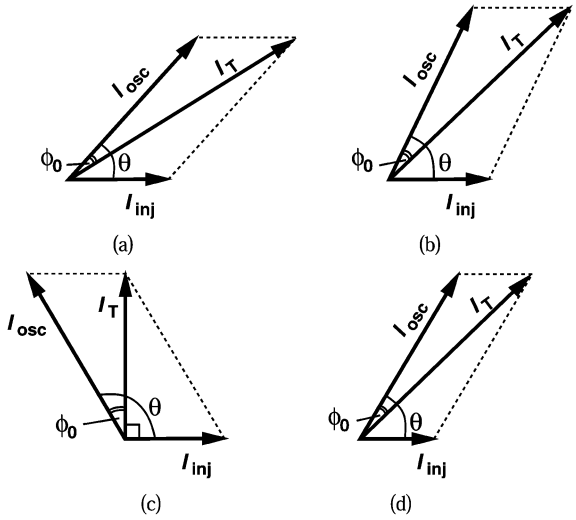

Fig. 3. Phase difference between input and output for different values of $|\omega_{\rm inj} - \omega_0|$ and $I_{\rm inj}$.

which reaches a maximum of

$$\sin\phi_{0,\max} = \frac{I_{\rm inj}}{I_{\rm osc}} \tag{3}$$

if

$$\cos\theta = -\frac{I_{\rm inj}}{I_{\rm osc}}. \tag{4}$$

Depicted in Fig. 3(c), these conditions translate to a 90° angle between the resultant and $I_{\rm inj}$, implying that the phase difference between the "input," $I_{\rm inj}$, and the output, $V_{\rm out}$, reaches a maximum of $90° + \phi_{0,\max}$. To compute the value of $\omega_{\rm inj}$ corresponding to this case, we first note that the phase shift of the tank in the vicinity of resonance is given by (Section III-A)

$$\tan\alpha \approx \frac{2Q}{\omega_0}(\omega_0 - \omega_{\rm inj}) \tag{5}$$

and recognize from Fig. 3(c) that $\tan\phi_0 = I_{\rm inj}/I_T$ and $I_T = \sqrt{I_{\rm osc}^2 - I_{\rm inj}^2}$. It follows that

$$\omega_0 - \omega_{\rm inj} = \frac{\omega_0}{2Q}\cdot\frac{I_{\rm inj}}{I_{\rm osc}}\cdot\frac{1}{\sqrt{1 - \dfrac{I_{\rm inj}^2}{I_{\rm osc}^2}}}. \tag{6}$$

(This result is obtained in [3] using a different approach.) We denote this maximum difference by ω_L, with the understanding that the overall lock range is in fact $\pm\omega_L$ around ω_0.[1]

The dependence of the lock range upon the injection level, $I_{\rm inj}$, is to be expected: if $I_{\rm inj}$ decreases, $I_{\rm osc}$ must form a *greater* angle with $I_{\rm inj}$ so as to maintain the phase difference between I_T and $I_{\rm osc}$ at ϕ_0 [Fig. 3(d)]. Thus, the circuit moves closer to the edge of the lock range.

As a special case, if $I_{\rm inj} \ll I_{\rm osc}$, then (2) reduces to

$$\sin\phi_0 \approx \frac{I_{\rm inj}}{I_{\rm osc}}\sin\theta \tag{7}$$

[1]We call ω_L the "one-sided" lock range.

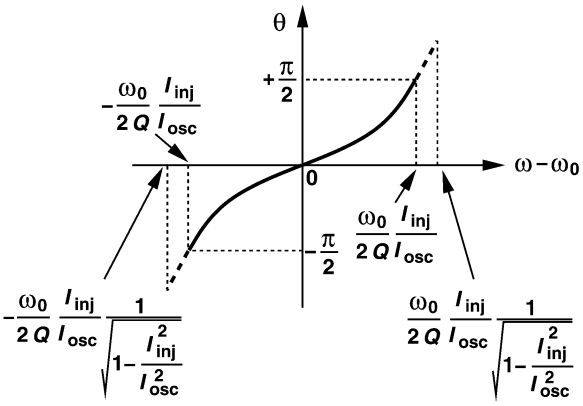

Fig. 4. Phase shift in an injection-locked oscillator.

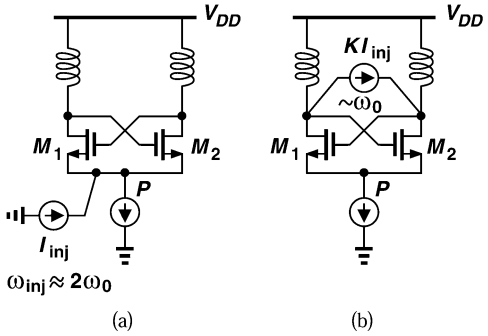

Fig. 5. (a) Injection-locked divider. (b) Equivalent circuit.

implying that ϕ_0 is small and $\sin\phi_0 \approx \tan\phi_0$. Equations (5) and (7) therefore give

$$\sin\theta \approx \frac{2Q}{\omega_0} \cdot \frac{I_{\rm osc}}{I_{\rm inj}}(\omega_0 - \omega_{\rm inj}) \tag{8}$$

for the input-output phase difference across the lock range. As evident from Fig. 3(c), for $I_{\rm inj} \ll I_{\rm osc}$ this difference reaches 90° at the edge of the lock range, a plausible result because if the zero crossings of the input fall on the peaks of the output, little phase synchronization occurs. The lock range in this case can be obtained from (6) or (8):

$$\omega_L \approx \frac{\omega_0}{2Q} \cdot \frac{I_{\rm inj}}{I_{\rm osc}}. \tag{9}$$

The subtle difference between (6) and (9) plays a critical role in quadrature oscillators (as explained below).

Fig. 4 plots the input-output phase difference across the lock range. In contrast to phase-locking, injection locking to $\omega_{\rm inj} \neq \omega_0$ mandates operation away from the tank resonance.

1) Application to Quadrature Oscillators: With the aid of a feedback model [13] or a one-port model [14], it can be shown that "antiphase" (unilateral) coupling of two identical oscillators forces them to operate in quadrature. It can also be shown [14] that this type of coupling (injection locking) shifts the frequency from resonance so that each tank produces a phase shift of

$$\theta = \tan^{-1}\frac{I_{\rm inj}}{I_{\rm osc}} \tag{10}$$

where $I_{\rm inj}$ denotes the current injected by one oscillator into the other and $I_{\rm osc}$ is the current produced by the core of each oscillator. Use of (5) therefore gives the required frequency shift as

$$\Delta\omega = \frac{\omega_0}{2Q} \cdot \frac{I_{\rm inj}}{I_{\rm osc}}. \tag{11}$$

Interestingly, (9) would imply that each oscillator is pushed to the *edge* of the lock range, but (6) suggests that for, say, $I_{\rm inj}/I_{\rm osc} = 0.25$, the lock range exceeds (9) by 3.3%. In other words, for a 90° phase difference between its input and output, an injection-locked oscillator need not operate at the edge of the lock range.

2) Application to Dividers: Fig. 5(a) shows an injection-locked oscillator operating as a ÷2 stage [15]. While previous work has treated the circuit as a nonlinear function to derive the lock range [15], it is possible to adopt a *time-variant* view to simplify the analysis. Switching at a rate equal to the oscillation frequency, M_1 and M_2 form a mixer that translates $I_{\rm inj}$ to $\omega_{\rm osc} \pm \omega_{\rm inj}$, with the sum component suppressed by the tank selectivity. Thus, as depicted in Fig. 5(b), injection of $I_{\rm inj}$ at $\omega_{\rm inj}$ into node P is equivalent to injection of $KI_{\rm inj}$ (where K is the mixer conversion gain) at $\omega_{\rm osc} - \omega_{\rm inj}$ directly into the oscillator. If M_1 and M_2 switch abruptly and the capacitance at node P is neglected, then $K = 2/\pi$, and (9) can be written as

$$\omega_L \approx \frac{\omega_0}{2Q} \cdot \frac{2}{\pi} \cdot \frac{I_{\rm inj}}{I_{\rm osc}}. \tag{12}$$

If referred to the input, this range must be doubled:

$$\omega_{L,in} \approx \frac{\omega_0}{2Q} \cdot \frac{4}{\pi} \cdot \frac{I_{\rm inj}}{I_{\rm osc}}. \tag{13}$$

Confirmed by simulations, (13) represents the upper bound on the lock range of injection-locked dividers.

III. Injection Pulling

If the injected signal frequency lies out of, but not very far from the lock range, the oscillator is "pulled." We study this behavior by computing the output phase of an oscillator under low-level injection.

A. Phase Shift Through a Tank

For subsequent derivations, we need an expression for the phase shift introduced by a tank in the vicinity of resonance. A second-order parallel tank consisting of L, C, and R_P exhibits a phase shift of

$$\alpha = \frac{\pi}{2} - \tan^{-1}\left(\frac{L\omega}{R_P} \cdot \frac{\omega_0^2}{\omega_0^2 - \omega^2}\right). \tag{14}$$

Since $\omega_0^2 - \omega^2 \approx 2\omega_0(\omega_0 - \omega)$, $L\omega/R_P = 1/Q$, and $\pi/2 - \tan^{-1} x = \tan^{-1}(x^{-1})$, we have

$$\tan\alpha \approx \frac{2Q}{\omega_0}(\omega_0 - \omega). \tag{15}$$

If the current flowing through the tank contains phase modulation, i.e., $I_{\text{in}} = I_0\cos[\omega t + \psi(t)]$, then the phase shift can be obtained by replacing ω in (15) with the instantaneous input frequency, $\omega + d\psi/dt$:

$$\tan\alpha \approx \frac{2Q}{\omega_0}\left(\omega_0 - \omega - \frac{d\psi}{dt}\right). \tag{16}$$

Valid for narrow-band phase modulation (slowly-varying ψ), this approximation holds well for typical injection phenomena.

B. Oscillator Under Injection

Consider the feedback oscillatory system shown in Fig. 6, where the injection is modeled as an additive input. The output is represented by a phase-modulated signal having a carrier frequency of ω_{inj} (rather than ω_0). In other words, the output is assumed to track the input except for a (possibly time-varying) phase difference. This representation is justified later. The objective is to calculate $V_X = V_{\text{in}} + V_{\text{out}}$, subject it to the phase shift of the tank, and equate the result to V_{out}.

The output of the adder is equal to

$$V_X = V_{\text{inj},p}\cos\omega_{\text{inj}}t + V_{\text{osc},p}\cos(\omega_{\text{inj}}t + \theta) \tag{17}$$

$$= (V_{\text{inj},p} + V_{\text{osc},p}\cos\theta)\cos\omega_{\text{inj}}t - V_{\text{osc},p}\sin\theta\sin\omega_{\text{inj}}t. \tag{18}$$

The two terms in (18) cannot be separately subjected to the tank phase shift because phase quantities do not satisfy superposition here. Thus, the right-hand side must be converted to a single sinusoid. Factoring $V_{\text{inj},p} + V_{\text{osc},p}\cos\theta$ and defining

$$\tan\psi = \frac{V_{\text{osc},p}\sin\theta}{V_{\text{inj},p} + V_{\text{osc},p}\cos\theta} \tag{19}$$

we write

$$V_X = \frac{V_{\text{inj},p} + V_{\text{osc},p}\cos\theta}{\cos\psi}\cos(\omega_{\text{inj}}t + \psi). \tag{20}$$

Since $\cos\psi = (\sqrt{1+\tan^2\psi})^{-1}$ and $V_{\text{inj},p} \ll V_{\text{osc},p}$, we have $\cos\psi \approx (V_{\text{inj},p} + V_{\text{osc},p}\cos\theta)/\sqrt{V_{\text{osc},p}^2 + 2V_{\text{osc},p}V_{\text{inj},p}\cos\theta}$, and hence

$$V_X \approx \sqrt{V_{\text{osc},p}^2 + 2V_{\text{osc},p}V_{\text{inj},p}\cos\theta}\cos(\omega_{\text{inj}}t + \psi) \approx V_{\text{osc},p}\cos(\omega_{\text{inj}}t + \psi). \tag{21}$$

Upon traveling through the *LC* tank, this signal experiences a phase shift given by (16):

$$V_{\text{out}} \approx V_{\text{osc},p}\cos\left\{\omega_{\text{inj}}t + \psi + \tan^{-1}\left[\frac{2Q}{\omega_0}\left(\omega_0 - \omega_{\text{inj}} - \frac{d\psi}{dt}\right)\right]\right\}. \tag{22}$$

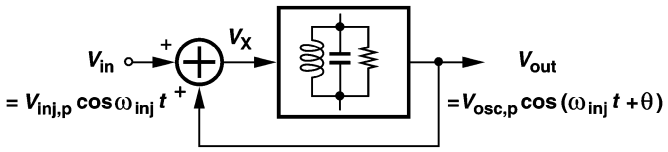

Fig. 6. *LC* oscillator under injection.

Equating this result to $V_{\text{osc},p}\cos(\omega_{\text{in}}t + \theta)$, we obtain

$$\psi + \tan^{-1}\left[\frac{2Q}{\omega_0}\left(\omega_0 - \omega_{\text{inj}} - \frac{d\psi}{dt}\right)\right] = \theta. \tag{23}$$

We also note from (19) that

$$\frac{d\psi}{dt} = \frac{V_{\text{osc},p}^2 + V_{\text{osc},p}V_{\text{inj},p}\cos\theta}{V_{\text{osc},p}^2 + 2V_{\text{osc},p}V_{\text{inj},p}\cos\theta + V_{\text{inj},p}^2}\frac{d\theta}{dt} \approx \frac{d\theta}{dt} \tag{24}$$

and

$$\tan(\theta - \psi) = \frac{V_{\text{inj},p}\sin\theta}{V_{\text{osc},p} + V_{\text{inj},p}\cos\theta} \tag{25}$$

$$\approx \frac{V_{\text{inj},p}}{V_{\text{osc},p}}\sin\theta. \tag{26}$$

It follows from (23), (24), and (26) that

$$\frac{d\theta}{dt} = \omega_0 - \omega_{\text{inj}} - \frac{\omega_0}{2Q}\cdot\frac{V_{\text{inj},p}}{V_{\text{osc},p}}\sin\theta \tag{27}$$

$$= \omega_0 - \omega_{\text{inj}} - \omega_L\sin\theta. \tag{28}$$

Originally derived by Adler [1] using a somewhat different approach, this equation serves as a versatile and powerful expression for the behavior of oscillators under injection.

Under locked condition, $d\theta/dt = 0$, yielding the same result as in (9) for the lock range. If $d\theta/dt \neq 0$, the equation must be solved to obtain the dependence of θ upon time. Note that $d\theta/dt$ is typically quite small because, from (28), it reaches a maximum of only $\omega_0 - \omega_{\text{inj}} + \omega_L \ll \omega_0$. That is, θ varies slowly under pulling conditions.

Adler's equation can be rewritten as

$$\frac{d\theta}{\omega_0 - \omega_{\text{inj}} - \omega_L\sin\theta} = dt. \tag{29}$$

Noting that $\sin\theta = 2\tan(\theta/2)/[1 + \tan^2(\theta/2)]$, making a change of variable $\tan(\theta/2) = u$, and carrying out the integration, we arrive at

$$\tan\frac{\theta}{2} = \frac{\omega_L}{\omega_0 - \omega_{\text{inj}}} + \frac{\omega_b}{\omega_0 - \omega_{\text{inj}}}\tan\frac{\omega_b t}{2} \tag{30}$$

where $\omega_b = \sqrt{(\omega_0 - \omega_{\text{inj}})^2 - \omega_L^2}$.[2] This paper introduces a graphical interpretation of this equation that confers insight into the phenomenon of injection pulling.

[2]Interestingly, ω_b is equal to the geometric mean of $\omega_0 + \omega_L - \omega_{\text{inj}}$ (the difference between ω_{inj} and the upper end of the lock range) and $\omega_0 - \omega_L - \omega_{\text{inj}}$ (the difference between ω_{inj} and the lower end of the lock range).

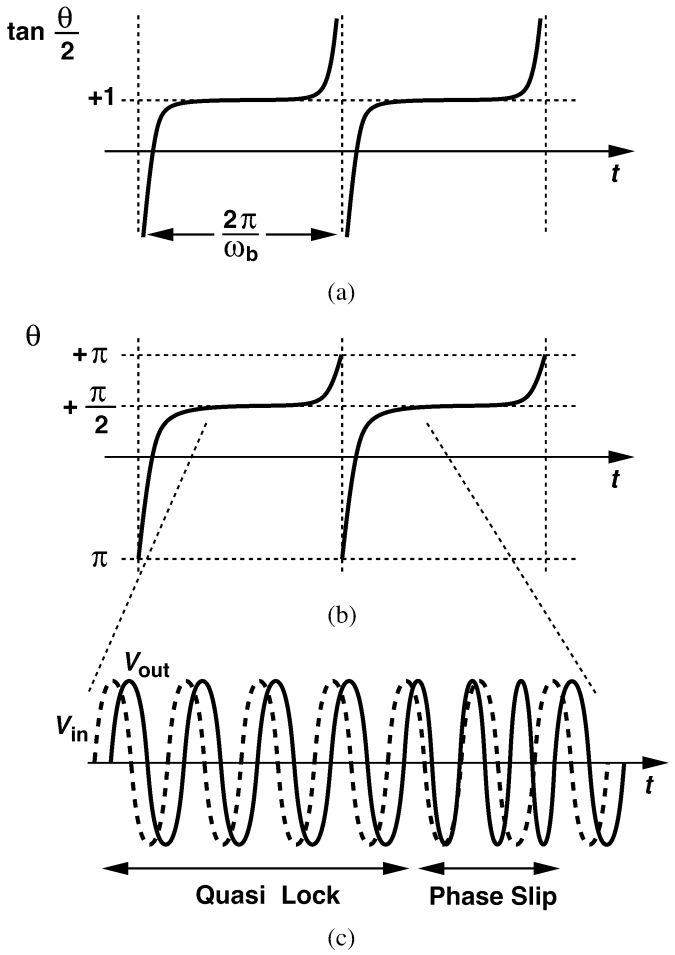

Fig. 7. Phase variation of an injection-pulled oscillator.

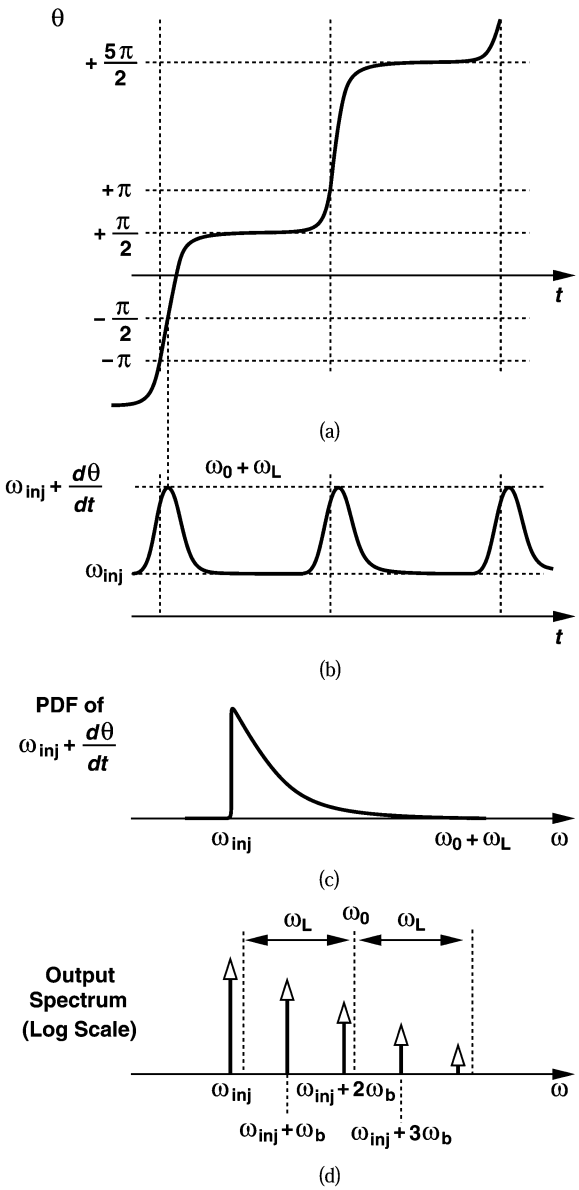

Fig. 8. Instantaneous frequency and spectrum of an injection-pulled oscillator.

C. Quasi-Lock

Let us first examine the above result for an input frequency just below the lock range, i.e., $\omega_{\rm inj} < \omega_0 - \omega_L$ but $(\omega_0 - \omega_{\rm inj})/\omega_L \approx 1$. Under this condition, ω_b is relatively small, and the right-hand side of (30) is dominated by the first term (≈ 1) so long as $\tan(\omega_b t/2)$ is less than one, approaching a large magnitude only for a short duration [Fig. 7(a)]. Noting that the cycle repeats with a period equal to ω_b, we plot θ as shown in Fig. 7(b). The key observation here is that θ is near 90° most of the time—as if the oscillator were injection-locked to the input at the edge of the lock range. At the end of each period and the beginning of the next period, θ undergoes a rapid 360° change and returns to the quasi-lock condition [Fig. 7(c)].

We now study the spectrum of the pulled oscillator. The spectrum has been analytically derived using different techniques [4], [5], but additional insight can be gained if the results in Fig. 7 are utilized as the starting point. The following observations can be made. 1) The periodic variation of θ at a rate of ω_b implies that the output beats with the input, exhibiting sidebands with a spacing of ω_b. Note that ω_b is a function of both $\omega_0 - \omega_{\rm inj}$ and ω_L (and hence the injection level). 2) Since the oscillator is almost injection-locked to the input for a large fraction of the period, we expect the spectrum to contain significant energy at $\omega_{\rm inj}$.

Redrawing Fig. 7(b) with the modulo-2π transitions at the end of each period removed [Fig. 8(a)] and writing the instantaneous frequency of the output as $d(\omega_{\rm inj}t + \theta)/dt = \omega_{\rm inj} + d\theta/dt$, we obtain the result depicted in Fig. 8(b). The interesting point here is that, for $\omega_{\rm inj}$ *below* the lock range, the instantaneous frequency of the oscillator goes only *above* $\omega_{\rm inj}$, exhibiting a peak value of $\omega_0 + \omega_L$ as obtained from (28). That is, the output spectrum contains mostly sidebands above $\omega_{\rm inj}$.

We now invoke a useful observation that the shape of the spectrum is given by the probability density function (PDF) of the instantaneous frequency [16]. The PDF is qualitatively plotted in Fig. 8(c), revealing that most of the energy is confined to the range $[\omega_{\rm inj}\ \omega_0 + \omega_L]$ and leading to the actual spectrum in Fig. 8(d). The magnitude of the sidebands drops approximately linearly on a logarithmic scale [4], [5].

Is it possible for one of the sidebands to fall at the natural frequency, ω_0? The following must hold: $\omega_0 = \omega_{\rm inj} + n\omega_b$, where n is an integer. Thus, $(\omega_0 - \omega_{\rm inj})^2/\omega_L^2 = 1 - 1/n^2$. Since $\omega_{\rm inj}$ is out of the lock range, the left side of this equation exceeds unity and no value of n can place a sideband at ω_0. We therefore say the oscillator is "pulled" from its natural frequency. This

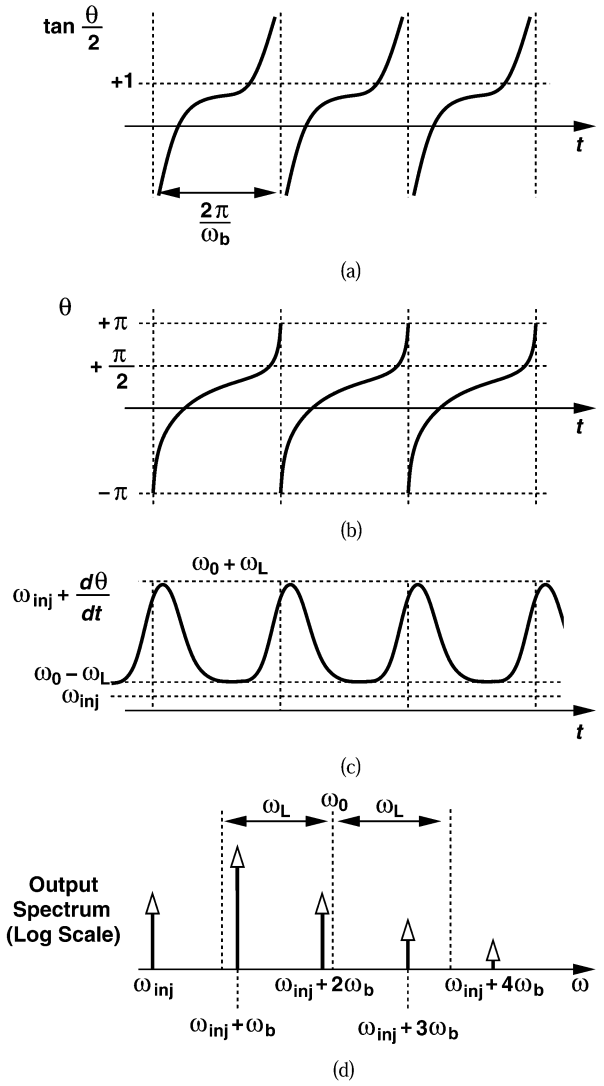

Fig. 9. Pulling behavior for injection somewhat far from the lock range.

also justifies the use of $\omega_{\rm inj}$—rather than ω_0—for the carrier frequency of the output in Fig. 6.

D. Fast Beat

It is instructive to examine the results obtained above as $\omega_{\rm inj}$ deviates farther from the lock range while other parameters remain constant. Rewriting (30) as

$$\tan\frac{\theta}{2}=\frac{\omega_L}{\omega_0-\omega_{\rm inj}}+\sqrt{1-\frac{\omega_L^2}{(\omega_0-\omega_{\rm inj})^2}}\tan\frac{\omega_b t}{2} \qquad (31)$$

we recognize that the vertical offset decreases whereas the slope of the second term increases. The right-hand side therefore appears as depicted in Fig. 9(a), yielding the behavior shown in Fig. 9(b) for θ. Thus, compared to the case illustrated in Fig. 7: 1) the beat frequency increases, leading to a wider separation of sidebands; 2) θ stays relatively constant for a shorter part of the period and exhibits a faster variation at the beginning and end; and 3) the instantaneous frequency is near $\omega_{\rm inj}$ for a shorter duration [Fig. 9(c)], producing a smaller spectral line at this frequency. In fact, if $\omega_{\rm inj}$ is sufficiently far from ω_0, the energy at

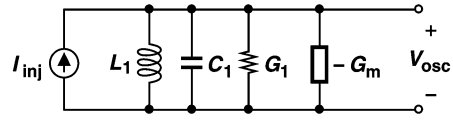

Fig. 10. One-port representation of an oscillator under injection.

$\omega_{\rm inj}$ falls below that at the next sideband $(\omega_{\rm inj}+\omega_b)$ [Fig. 9(d)]. Eventually, the components at $\omega_{\rm inj}$ and $\omega_{\rm inj}+2\omega_b$ have approximately equal levels [4], [5].

Interestingly, the analyses in [4] and [5] only reveal the spectrum in Fig. 9(d). On the other hand, the approach presented here, particularly the use of the PDF of the instantaneous frequency, correctly predicts both quasi-lock and fast beat conditions.

In quadrature oscillators, pulling may occur if the frequency mismatch between the two cores exceeds the injection lock range. With insufficient coupling, the oscillators display a behavior similar to that depicted in Figs. 7 and 9. Note that the resulting sidebands are *not* due to intermodulation between the two oscillator signals. For example, the spacing between the sidebands is a function of the coupling factor.

IV. Requisite Oscillator Nonlinearity

Our analysis of injection locking and pulling has thus far ignored nonlinearities in the oscillator. While this may imply that a "linear" oscillator[3] can be injection pulled or locked, we know from the superposition principle that this cannot happen. Specifically, a linear oscillator would simply generate a sinusoid at ω_0 in response to an initial condition and another at $\omega_{\rm inj}$ is response to the input. To resolve this paradox, we reexamine the oscillatory system under injection, seeking its envelope behavior.

In this case, it is simpler to model the oscillator as a one-port circuit consisting of a parallel tank and a mildly nonlinear negative conductance (Fig. 10), where G_1 represents the loss of the tank. For example, M_1 and the inverting buffer in Fig. 2(a) constitute a negative G_m cell. In this circuit

$$C_1\frac{d^2V_{\rm osc}}{dt^2}-(G_1-G_m)\frac{dV_{\rm osc}}{dt}+\frac{1}{L_1}V_{\rm osc}=\frac{dI_{\rm inj}}{dt}. \qquad (32)$$

Now let us assume $I_{\rm inj}(t)=I_{{\rm inj},p}\cos\omega_{\rm inj}t=\mathrm{Re}\{I_{{\rm inj},p}\exp(j\omega_{\rm inj}t)\}$ and $V_{\rm osc}(t)=V_{\rm env}(t)\cos(\omega_{\rm inj}t+\theta)=\mathrm{Re}\{V_{\rm env}(t)\exp(j\omega_{\rm inj}t+j\theta)\}$, where $V_{\rm env}(t)$ denotes the envelope of the output. Substituting the exponential terms in (32) and separating the real and imaginary parts, we have

$$\begin{aligned}&C_1\frac{d^2V_{\rm env}}{dt^2}-C_1\left(\omega_{\rm inj}+\frac{d\theta}{dt}\right)^2V_{\rm env}\\&\quad+(G_1-G_m)\frac{dV_{\rm env}}{dt}+\frac{1}{L_1}V_{\rm env}=\omega_{\rm inj}I_{{\rm inj},p}\sin\theta \qquad (33)\\&2C_1\left(\omega_{\rm inj}+\frac{d\theta}{dt}\right)\frac{dV_{\rm env}}{dt}+C_1\frac{d^2\theta}{dt^2}V_{\rm env}\\&\quad+(G_1-G_m)\left(\omega_{\rm inj}+\frac{d\theta}{dt}\right)V_{\rm env}=\omega_{\rm inj}I_{{\rm inj},p}\cos\theta. \qquad (34)\end{aligned}$$

[3]A linear oscillator can be defined as one in which the loop gain is exactly unity for all signal levels.

To simplify these equations, we assume: 1) the envelope varies slowly and by a small amount; 2) the magnitude of the envelope can be approximated as the tank peak current produced by the $-G_m$ circuit, $I_{\text{osc},p}$, multiplied by the tank resistance $R_P = G^{-1} = QL_1\omega_0$; 3) $\omega_{\text{inj}}^2 - \omega_0^2 \approx 2\omega_0(\omega_0 - \omega_{\text{inj}})$; 4) $\omega_{\text{inj}} \approx \omega_0$ where applicable; and 5) the phase and its derivatives vary slowly. Equations (33) and (34) thus reduce to

$$\frac{d\theta}{dt} = \omega_0 - \omega_{\text{inj}} - \frac{\omega_0 I_{\text{inj},p}}{2QI_{\text{osc},p}} \sin\theta \tag{35}$$

$$\frac{dV_{\text{env}}}{dt} + \frac{G_1 - G_m}{2C_1} V_{\text{env}} = \frac{I_{\text{inj},p}\cos\theta}{2C_1}. \tag{36}$$

The first is Adler's equation, whereas the second expresses the behavior of the envelope.

To develop more insight, let us study these results within the lock range, i.e., if $d\theta/dt = dV_{\text{env}}/dt = 0$. Writing $\sin^2\theta + \cos^2\theta = 1$ gives the following useful identity:

$$\left(\frac{\omega_0 - \omega_{\text{inj}}}{\omega_L}\right)^2 + \left(\frac{G_1 - G_m}{I_{\text{inj},p}} V_{\text{env},p}\right)^2 = 1. \tag{37}$$

For $\omega_{\text{inj}} = \omega_0$

$$G_m = G_1 - \frac{I_{\text{inj},p}}{V_{\text{env},p}} \tag{38}$$

that is, the circuit responds by *weakening* the $-G_m$ circuit (i.e., allowing more saturation) because the injection adds in-phase energy to the oscillator. On the other hand, for $|\omega_0 - \omega_{\text{inj}}| = \omega_L$, we have $G_m = G_1$, as if there is no injection. Fig. 11 illustrates the behavior of G_m across the lock range.

While derived for a mildly-nonlinear oscillator, the above result does suggest a general effect: the oscillator must spend less time in the linear regime as ω_{inj} moves closer to ω_0. A "linear" oscillator therefore does not injection lock.

V. Phase Noise

The phase noise of oscillators can be reduced by injection locking to a low-noise source. From a time-domain perspective, the "synchronizing" effect of injection manifests itself as correction of the oscillator zero crossings in every period, thereby lowering the accumulation of jitter. This viewpoint also reveals that the reduction of phase noise depends on the injection level, and it reaches a maximum for $\omega_{\text{inj}} = \omega_0$ [Fig. 12(a)] (where the zero crossings of I_{inj} greatly impact those of I_{osc}) and a minimum for $\omega_{\text{inj}} = \omega_0 \pm \omega_L$ [Fig. 12(b)] (where the zero crossings of I_{inj} coincide with the zero-slope points on I_{osc}).

Using the one-port model of Fig. 10 and the identity expressed by (38), we can estimate the phase noise reduction in a mildly nonlinear oscillator that is injection-locked to a noiseless source. As depicted in Fig. 13, the noise of the tank and the $-G_m$ cell can be represented as a current source I_n. In the absence of injection, the (average) value of $-G_m$ cancels G_1, and I_n experiences the following transimpedance:

$$\left|\frac{V_{\text{out}}}{I_n}(j\omega_n)\right| \approx \frac{1}{|2(\omega_n - \omega_0)C_1|}. \tag{39}$$

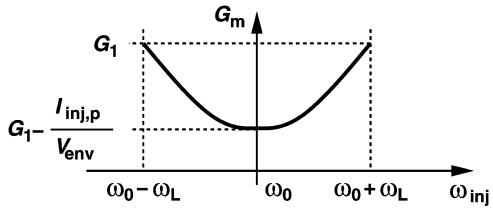

Fig. 11. Variation of G_m across the lock range.

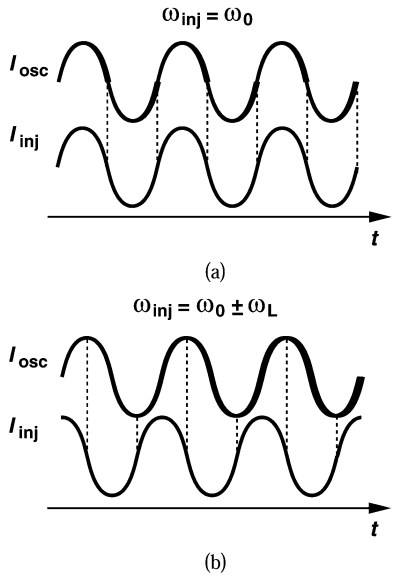

Fig. 12. Conceptual illustration of effect of injection locking on jitter (a) in the middle and (b) at the edge of the lock range.

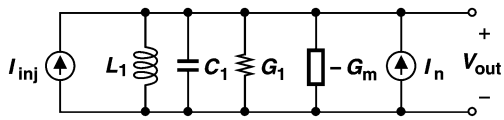

Fig. 13. Model for studying phase noise.

Thus, I_n is amplified by an increasingly higher gain as the noise frequency approaches ω_0.[4]

Now suppose a finite injection is applied at the center of the lock range, $\omega_{\text{inj}} = \omega_0$. Then, (38) predicts that the overall tank admittance rises to $G_1 - G_m = I_{\text{inj},p}/V_{\text{env},p}$. In other words, the tank impedance seen by I_n at ω_0 falls from infinity (with no injection) to $V_{\text{env},p}/I_{\text{inj},p}$ under injection locking. As the frequency of I_n deviates from ω_0, $V_{\text{env},p}/I_{\text{inj},p}$ continues to dominate the tank impedance up to the frequency offset at which the phase noise approaches that of the free-running oscillator (Fig. 14). To determine this point, we equate the free-running noise shaping function of (39) to $V_{\text{env},p}/I_{\text{inj},p}$ and note that $C_1/G_1 = Q/\omega_0$ and $V_{\text{env},p} \approx I_{\text{osc},p}/G_1$:

$$|\omega_n - \omega_0| = \frac{\omega_0}{2Q} \cdot \frac{I_{\text{inj},p}}{I_{\text{osc},p}}. \tag{40}$$

Thus, the free-running and locked phase noise profiles meet at the edges of the lock range.

[4]For very small frequency offsets, the noise shaping function assumes a Lorentzian shape and hence a finite value.

As illustrated in Fig. 12(b), if the input frequency deviates from ω_0, the resulting phase noise reduction becomes less pronounced. In fact, as $\omega_{\rm inj}$ approaches either edge of the lock range, $G_1 - G_m$ drops to zero, raising the impedance seen by the noise current.

In CMOS technology, it is difficult to rely on the phase noise reduction property of injection locking. Since the lock range is typically quite narrow and since the natural frequency of oscillators incurs significant error due to process variations and poor modeling, the locking may occur near the edge of the lock range, thereby lowering the phase noise only slightly. For example, if the two-sided lock range is equal to $\pm 5\%$ and the natural frequency of the oscillator varies by $\pm 4\%$ with process and temperature, then, in the worst case, the injection locking occurs at $\omega_0 - \omega_{\rm inj} = 0.8\omega_L$. It follows from (37) and the above observations that the impedance seen by the noise falls from infinity to $1.67\, V_{{\rm env},p}/I_{{\rm inj},p}$, yielding a 4.4-dB degradation in the phase noise compared to the case of $\omega_0 - \omega_{\rm inj} = 0$.

VI. Injection Pulling in Phase-Locked Oscillators

The analysis in Section III deals with pulling in nominally free-running oscillators, a rare case of practical interest. Since oscillators are usually phase-locked, the analysis must account for the correction poduced by the PLL. In this section, we assume the oscillator is pulled by a component at $\omega_{\rm inj}$ while phase-locked so as to operate at ω_0. We also assume that the oscillator control has a gain of $K_{\rm VCO}$ and contains a small perturbation, $V_{\rm cont}$, around a dc level.

Examining the derivations in Section III for a VCO, we observe that (19) and (21) remain unchanged. In (22), on the other hand, we must now add $K_{\rm VCO}V_{\rm cont}$ to ω_0. For small perturbations, $K_{\rm VCO}V_{\rm cont}$ can be neglected in the denominator of $2Q/\omega_0$ and

$$V_{\rm out} = V_{{\rm osc},p}\cos\left\{\omega_{\rm inj}t + \psi + \tan^{-1}\left[\frac{2Q}{\omega_0}\left(\omega_0 + K_{\rm VCO}V_{\rm cont} - \omega_{\rm inj} - \frac{d\psi}{dt}\right)\right]\right\}. \quad (41)$$

Equating the phase of (41) to $\omega_{\rm inj}t + \theta$ and noting that (24) and (26) can be shown to still hold, we have

$$\frac{d\theta}{dt} = \omega_0 + K_{\rm VCO}V_{\rm cont} - \omega_{\rm inj} - \omega_L\sin\theta. \quad (42)$$

Fig. 15 shows a PLL consisting of a phase/frequency detector (PFD), a charge pump (CP), and a low-pass filter (R_P and C_P), and the VCO under injection. Since with a low injection level, the PLL remains phase-locked to ω_0, it is more meaningful to express the output phase as $\omega_0 t + \phi$ rather than $\omega_{\rm inj}t + \theta$. Thus, $\omega_{\rm inj} + d\theta/dt = \omega_0 + d\phi/dt$ and

$$\frac{d\phi}{dt} = K_{\rm VCO}V_{\rm cont} - \omega_L\sin[\phi - (\omega_{\rm inj} - \omega_0)t] \quad (43)$$

$$\approx K_{\rm VCO}V_{\rm cont} + \omega_L\sin(\omega_{\rm inj} - \omega_0)t \quad (44)$$

where it is assumed $\phi \ll 1$ radian. This approximation is reasonable if pulling does not excessively corrupt the PLL output.

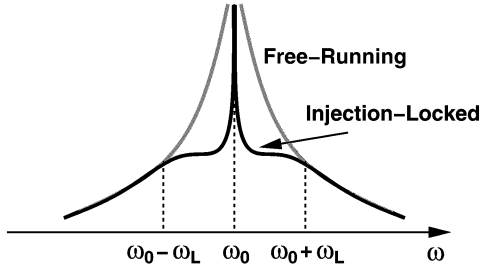

Fig. 14. Reduction of phase noise due to injection locking.

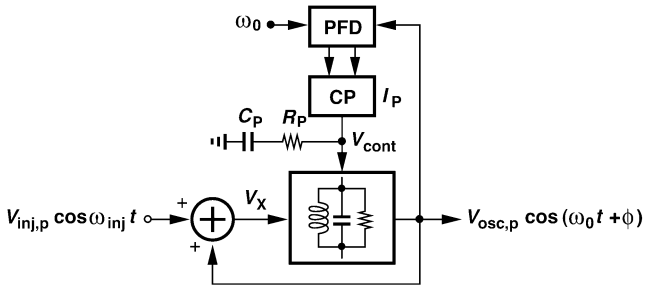

Fig. 15. PLL under injection pulling.

The above result can now be used in a PLL environment. In Fig. 15, the PFD, CP, and loop filter collectively provide the following transfer function:

$$\frac{V_{\rm cont}}{\Phi}(s) = -\frac{I_P}{2\pi}\left(R_P + \frac{1}{C_P s}\right) \quad (45)$$

where the negative sign accounts for phase subtraction by the PFD. We therefore have

$$V_{\rm cont}(t) = -\frac{I_P R_P}{2\pi}\phi(t) - \frac{I_P}{2\pi C_P}\int \phi(t)\, dt. \quad (46)$$

Substituting for $V_{\rm cont}$ in (44) and differentiating both sides with respect to time, we obtain

$$\frac{d^2\phi}{dt^2} + K_{\rm VCO}\frac{I_P R_P}{2\pi}\frac{d\phi}{dt} + K_{\rm VCO}\frac{I_P}{2\pi C_P}\phi = \omega_L\Delta\omega\cos\Delta\omega t \quad (47)$$

where $\Delta\omega = \omega_{\rm inj} - \omega_0$. This reveals that the PLL behaves as a second-order system in its response to injection pulling. Defining

$$\zeta = \frac{R_P}{2}\sqrt{\frac{I_P K_{\rm VCO}C_P}{2\pi}} \quad (48)$$

$$\omega_n = \sqrt{\frac{I_P K_{\rm VCO}}{2\pi C_P}} \quad (49)$$

we have

$$\phi(t) = \frac{\omega_L\Delta\omega}{\sqrt{(\Delta\omega^2 - \omega_n^2)^2 + 4\zeta^2\omega_n^2\Delta\omega^2}}\cos(\Delta\omega t - \beta) \quad (50)$$

where β denotes the phase of the transfer function at a frequency of $\Delta\omega$.[5]

[5]A dual-loop model developed by A. Mirzaei arrives at a similar result but with a different value for the peak amplitude of the cosine [17].

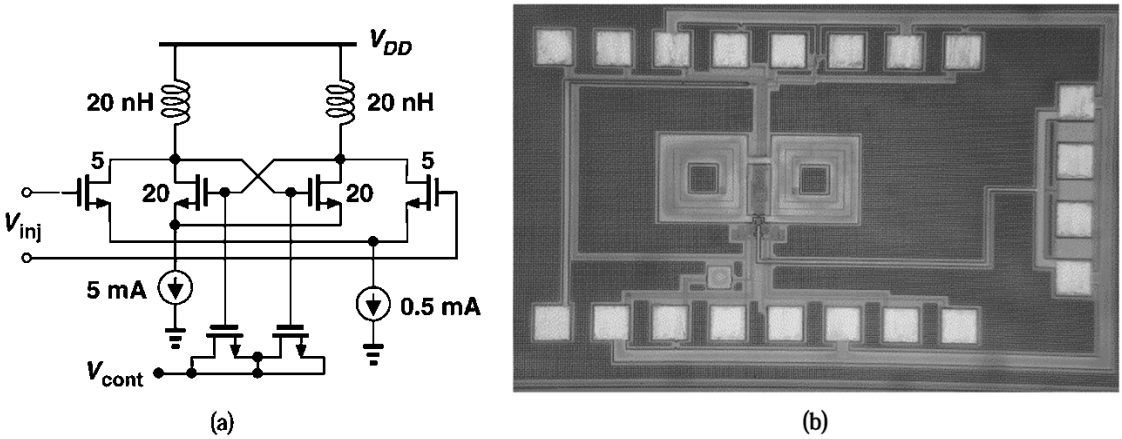

Fig. 16. (a) *LC* VCO. (b) Die photograph.

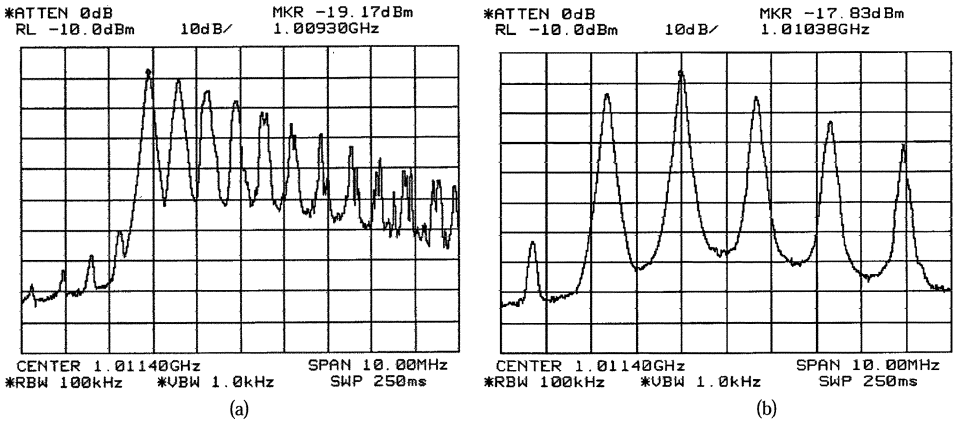

Fig. 17. Measured spectrum of free-running oscillator under injection. (a) Quasi-lock. (b) Fast beat.

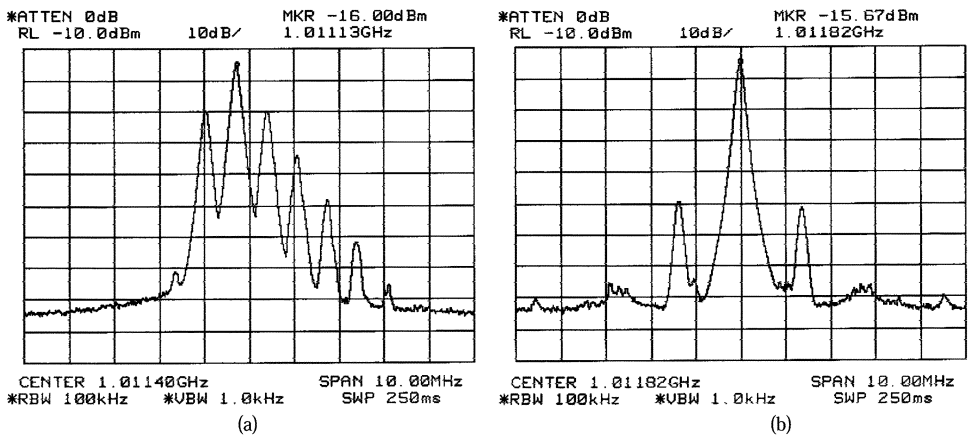

Fig. 18. Measured spectrum of (a) free-running oscillator under injection, and (b) phase-locked oscillator under injection.

Equation (50) leads to several interesting and important observations. First, the VCO output phase is modulated *sinusoidally*, thereby creating only two symmetric sidebands (for low injection). The sidebands reside at $\omega_0 \pm \Delta\omega$, i.e., at $\omega_{\rm inj}$ and $2\omega_0 - \omega_{\rm inj}$. Second, (46) suggests that the control voltage also varies sinusoidally at a frequency of $\Delta\omega$, possibly serving as a point for monitoring the strength of pulling. Third, the peak value of ϕ in (50) and hence the sideband magnitudes vary with $\Delta\omega$; in fact, they approach zero for both $\Delta\omega \to 0$ and $\Delta\omega \to \infty$, assuming a peak in between. This is because the PLL suppresses the effect of pulling if $\omega_{\rm inj} - \omega_0$ is well within the loop bandwidth and the oscillator pulling becomes less significant if $\omega_{\rm inj} - \omega_0$ is large.

The bandpass behavior of the peak phase in (50) stands in sharp contrast to the response of PLLs to *additive* phase at the output of the VCO. For example, the VCO phase noise experiences a high-pass transfer to the output.

The symmetry of sidebands can also be interpreted with the aid of the relationship between the shape of the spectrum and the PDF of the instantaneous frequency, $f_{\rm inst}$. If the sidebands were

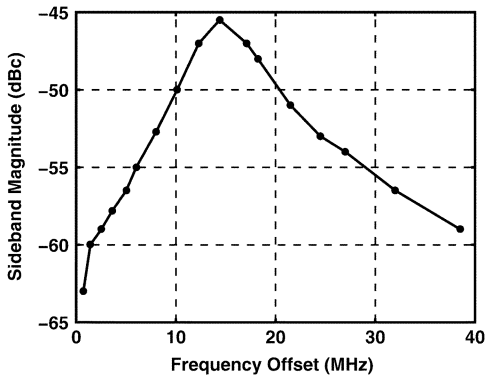

Fig. 19. Measured profile of sidebands.

asymmteric, so would the PDF of $f_{\rm inst}$ be. That is, $f_{\rm inst}$ would spend more time at one of its extremes. The PLL would then apply a greater correction at that extreme, eventually creating a symmetric spectrum.

The foregoing analysis assumes a first-order loop filter and continuous-time loop operation. The addition of a second capacitor from the oscillator control line to ground and the discrete-time nature of the loop lead to sideband magnitudes that are somewhat different from those predicted by (50). For this reason, circuit simulations are often necessary to determine the sideband levels accurately.

VII. Experimental Results

A 1-GHz charge-pump phase-locked loop including a $\div 4$ circuit has been designed and fabricated in 0.35-μm CMOS technology. Fig. 16(a) shows the *LC* oscillator and the method of injection, with the transistor widths shown in microns (the lengths are equal to 0.35 μm), and Fig. 16(b) depicts the die photo.

The distinction between quasi-lock and fast beat cases is demonstrated in the spectra of Fig. 17 for the free-running oscillator. Here, the injected level is approximately 38 dB below the oscillation level[6] and the lock range is equal to ± 1.5 MHz. Indeed, for injection 110 kHz outside the lock range, [Fig. 17(a)], the sideband at $\omega_{\rm inj}$ displays the largest magnitude. As $\omega_{\rm inj}$ further deviates from the lock range (710 kHz outside the lock range), the component at $\omega_{\rm inj} + \omega_b$ becomes dominant.

Fig. 18(a) and (b) compares the output spectrum before and after phase-locking, respectively. Here, the injected level is approximately 53 dB below the oscillation level. As the analysis in Section III predicts, the sidebands become symmetric after the loop is closed. The left sideband in Fig. 18(b) is located at $\omega_{\rm inj}$ and is slightly larger than the right one. This is because $\omega_{\rm inj}$ also feeds through the oscillator to the output. In other words, if $\omega_{\rm inj}$ is moved to above ω_0, then the right sideband becomes larger. Measurements also confirm that the spectrum remains symmetric even for a very small charge pump current—but the sidebands rise in both magnitude and number.

Fig. 19 plots the profile of the sidebands as $\omega_{\rm inj}$ varies from ω_0 to large values, confirming the bandpass behavior of pulling. These results agree well with simulations. The theoretical predictions overestimate the peak of this profile by about 7 dB.

[6]This is derived from the measured lock range: $I_{\rm inj}/I_{\rm osc} = 2Q(\omega_L/\omega_0)$.

References

[1] R. Adler, "A study of locking phenomena in oscillators," *Proc. IEEE*, vol. 61, pp. 1380–1385, Oct. 1973.
[2] K. Kurokawa, "Injection locking of microwave solid-state oscillators," *Proc. IEEE*, vol. 61, pp. 1336–1410, Oct. 1973.
[3] L. J. Paciorek, "Injection locking of oscillators," *Proc. IEEE*, vol. 53, pp. 1723–1727, Nov. 1965.
[4] H. L. Stover, "Theoretical explanation of the output spectra of unlocked driven oscillators," *Proc. IEEE*, vol. 54, pp. 310–311, Feb. 1966.
[5] M. Armand, "On the output spectrum of unlocked driven oscillators," *Proc. IEEE*, vol. 59, pp. 798–799, May 1969.
[6] A. E. Siegman, *Lasers*. Mill Valley, CA: University Science Books, 1986.
[7] R. R. Ward, *The Living Clocks*. New York: Alfred Knopf, 1971.
[8] V. Manassewitsch, *Frequency Synthesizers*, 3rd ed. New York: Wiley, 1987.
[9] E. Normann, "The inductance-capacitance oscillator as a frequency divider," in *Proc. IRE*, vol. 24, Oct. 1946, pp. 799–803.
[10] C. J. M. Verhoeven, "A high-frequency electronically tunable quadrature oscillator," *IEEE J. Solid-State Circuits*, vol. 27, pp. 1097–1100, July 1992.
[11] A. Rofougaran *et al.*, "A 900 MHz CMOS LC oscillator with quadrature outputs," in *IEEE ISSCC Dig. Tech. Papers*, Feb. 1996, pp. 392–393.
[12] J. Kim and B. Kim, "A low phase noise CMOS LC oscillator with a ring structure," in *IEEE ISSCC Dig. Tech. Papers*, Feb. 2000, pp. 430–431.
[13] T. P. Liu, "A 6.5 GHz monolithic CMOS voltage-controlled oscillator," in *IEEE ISSCC Dig. Tech. Papers*, Feb. 1999, pp. 404–405.
[14] B. Razavi, *Design of Integrated Circuits for Optical Communications*. New York: McGraw-Hill, 2002.
[15] H. R. Rategh and T. H. Lee, "Superharmonic injection-locked frequency dividers," *IEEE J. Solid-State Circuits*, vol. 34, pp. 813–821, June 1999.
[16] H. E. Rowe, *Signals and Noise in Communication Systems*. Princeton, NJ: Van Nostrand, 1965.
[17] A. Mirzaei, private communication.

Behzad Razavi (S'87–M'90–SM'00–F'03) received the B.Sc. degree in electrical engineering from Sharif University of Technology, Tehran, Iran, in 1985 and the M.Sc. and Ph.D. degrees in electrical engineering from Stanford University, Stanford, CA, in 1988 and 1992, respectively.

He was an Adjunct Professor at Princeton University, Princeton, NJ, from 1992 to 1994, and at Stanford University, Stanford, CA, in 1995. He was with AT&T Bell Laboratories and Hewlett-Packard Laboratories until 1996. Since 1996, he has been Associate Professor and subsequently Professor of electrical engineering at the University of California, Los Angeles. He si the author of *Principles of Data Conversion System Design* (IEEE Press, 1995), *RF Microelectronics* (Prentice Hall, 1998) (also translated into Japanese), *Design of Analog CMOS Integrated Circuits* (McGraw-Hill, 2001) (also translated into Chinese and Japanese), and *Design of Integrated Circuits for Optical Communications* (McGraw-Hill, 2003), and the editor of *Monolithic Phase-Locked Loops and Clock Recovery Circuits* (IEEE Press, 1996), and *Phase-Locking in High-Performance Systems* (IEEE Press, 2003). His current research includes wireless transceivers, frequency synthesizers, phase locking and clock recovery for high-speed data communications, and data converters.

Dr. Razavi received the Beatrice Winner Award for Editorial Excellence at the 1994 IEEE International Solid-State Circuits Conference (ISSCC), the best paper award at the 1994 European Solid-State Circuits Conference, the Best Panel Award at the 1995 and 1997 ISSCC, the TRW Innovative Teaching Award in 1997, and the Best Paper Award at the IEEE Custom Integrated Circuits Conference in 1998. He was the co-recipient of both the Jack Kilby Outstanding Student Paper Award and the Beatrice Winner Award for Editorial Excellence at the 2001 ISSCC. He has been recognized as one of the top ten authors in the 50-year history of ISSCC. He served on the Technical Program Committees of the ISSCC from 1993 to 2002 and the VLSI Circuits Symposium from 1998 to 2002. He has also served as Guest Editor and Associate Editor of the IEEE JOURNAL OF SOLID-STATE CIRCUITS, IEEE TRANSACTIONS ON CIRCUITS AND SYSTEMS, and the *International Journal of High Speed Electronics*. He is an IEEE Distinguished Lecturer.